Origin of Transitions Inversion in Rare-Earth Vanadates

Xue-Jing Zhang, 1 Erik Koch, 2 and Eva Pavarini 1 ¹Peter Grünberg Institute, Forschungszentrum Jülich, 52425 Jülich, Germany ²Jülich Supercomputing Centre, Forschungszentrum Jülich, 52425 Jülich, Germany

(Received 25 October 2024; revised 31 January 2025; accepted 25 June 2025; published 11 July 2025)

In correlated transition-metal oxides, orbital-ordering appears to always precede magnetic ordering $(T_N < T_{OO})$. The RVO₃ series is the exception: it exhibits an inversion of T_N and T_{OO} with increasing rareearth radius R_I . Why vanadates are different is not understood. Here we show that the reason is fundamental: when lattice effects dominate orbital physics, magnetic order follows orbital order, and thus $T_N < T_{\rm OO}$. This is what happens in most transition-metal oxides, and it is what quenches exotic quantum orbital phases. In the RVO₃ series, however, lattice effects become ineffective with increasing R_I , while, at the same time, for antiferromagnetic spin order, the orbital-independent dipolar spin-spin interaction dominates. This has consequences well beyond the RVO3 series itself. In fact, the subtle balance of interactions leading to the T_N - T_{OO} inversion not only explains why it is so rare, but also gives the criteria for finding it in other materials. The mechanism behind transitions inversion makes such systems an ideal playground for studying unconventional orbital phases. The results presented here rely on the decomposition of the order parameter into irreducible tensors, which allows us to identify the mechanism driving the transition.

DOI: 10.1103/qvp2-jn9p

Introduction—The interplay of the spin, orbital, and lattice degrees of freedom in strongly correlated transitionmetal oxides results in a plethora of phenomena of puzzling complexity [1–3]. In recent years, heterostructuring, disorder and nonequilibrium techniques [4–6] have opened the path to discovering or engineering new phases. In this panorama, the series of t_{2a}^2 perovskites RVO₃ (where R is a rare earth) is paradigmatic [7–27]. In fact, these systems exhibit a set of different phases, structural and electronic, whose onset depends on the rare-earth radius R_I . They are orthorhombic GdFeO3-type at high temperature and become monoclinic at a temperature T_S ; the orthorhombic phase is, however, either reentrant at $T_{S'} < T_S$ (small R_I), or coexists with the monoclinic phase in a large temperature window (e.g., for intermediate R_I) [12,20]. Structural changes have been identified with changes in orbital ordering (OO).

The truly peculiar aspect of the phase diagram, however, is the reversal of the spin- and orbital-ordering transition with increasing R_I . In correlated transition-metal oxides, the magnetic transition appears to always occur below the orbital ordering transition ($T_N < T_{OO}$). In the vanadates, surprisingly, this classic scenario is only found for small R_I ;

Published by the American Physical Society under the terms of the Creative Commons Attribution 4.0 International license. Further distribution of this work must maintain attribution to the author(s) and the published article's title, journal citation, and DOI.

in this case, the antiferro (AF) magnetic transition occurs in fact at $T_{\rm N} < T_{\rm S}$ [20–25], when orbital fluctuations are already suppressed [28–30], i.e., $T_{OO} > T_{S} > T_{N}$. Yet, increasing R_I , the magnetic and orbital transition approach each other $(T_N \to T_{OO})$, eventually inverting [25–27]. The complex phase diagram of the RVO₃ series is believed to be the result of the interplay of lattice distortion, leading to a sizable intra- t_{2q} crystal-field (CF) splitting, and superexchange (SE) effects of the Kugel' and Khomskii (KK) type [31]. Indeed, we recently have identified LaVO₃ as an orbitally ordered system of the KK kind [32]. What, however, is responsible for the surprising inversion of

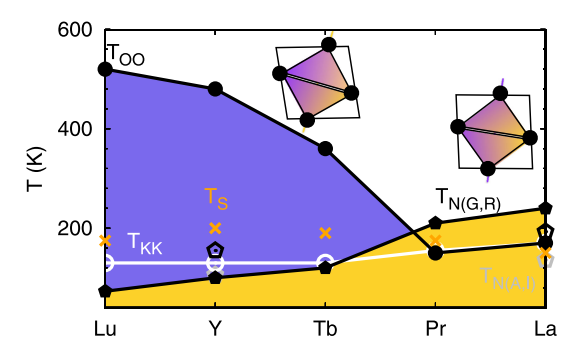


FIG. 1. T_N - T_{OO} inversion with increasing R_I . Black circles: orbital-ordering temperature $T_{\rm OO}$. White circles: Kugel-Khomskii superexchange transition temperature $T_{\rm KK}$. Pentagons: AFmagnetic transition temperature T_N [G-type (black) and A-type (gray)]. R: real structure. I: idealized case with zero CF. T_S : experimental structural transition [25].

 T_N and T_{OO} with increasing R_I , and why only in the vanadates, is not understood.

In this Letter we address and solve this problem. We show that the inversion is the result of an unusual balance of interactions. When R_I is small, lattice distortions suppress the most efficient orbital SE channels. This leads to the "classical" picture [33–37] with $T_N < T_{OO}$, because the orbital state is determined by the CF splitting. Increasing R_I , however, reinforces xz-xz quadrupolar SE, which, eventually, drives orbital physics; yet, antiferro (AF) spin-spin interactions grow as well, while, at the same time, orbital SE terms of different spin rank compete. In the end, the energy balance tilts, leading to magnetic ordering preceding OO. The resulting phase diagram is shown schematically in Fig. 1.

Model and method—We adopt the local-density approximation + dynamical mean-field theory (LDA+DMFT) approach. First we perform local-density-approximation calculations using the full-potential linearized augmented plane-wave method as implemented in the WIEN2K code [38]. Next we construct Wannier functions spanning the t_{2g} bands using the maximal localization procedure [39,40]. Finally, we build the associated Hubbard model

$$\begin{split} \hat{H} &= -\sum_{ii'\sigma} \sum_{mm'} t_{mm'}^{i,i'} c_{im\sigma}^{\dagger} c_{i'm'\sigma} + U \sum_{im} \hat{n}_{im\uparrow} \hat{n}_{im\downarrow} \\ &+ \frac{1}{2} \sum_{i\sigma\sigma'} \sum_{m \neq m'} (U - 2J - J \delta_{\sigma,\sigma'}) \hat{n}_{im\sigma} \hat{n}_{im'\sigma'} \\ &- J \sum_{im \neq m'} (c_{im\uparrow}^{\dagger} c_{im\downarrow}^{\dagger} c_{im'\uparrow} c_{im'\downarrow} + c_{im\uparrow}^{\dagger} c_{im\downarrow} c_{im'\downarrow}^{\dagger} c_{im'\uparrow}). \end{split}$$

$$(1)$$

Here $t_{mm'}^{i,i'}$ is the hopping integral from orbital m on site i to orbital m' on site i'; $\varepsilon_{mm'}^{i,i} = -t_{mm'}^{i,i}$ is the crystal-field matrix. The operator $c_{im\sigma}^{\dagger}\left(c_{im\sigma}\right)$ creates (annihilates) an electron with spin σ in Wannier state m at site i and $\hat{n}_{im\sigma} = c_{im\sigma}^{\dagger} c_{im\sigma}$. The screened Coulomb parameters are U = 5 eV and J = 0.68 eV, established values for these systems [29,41,42]. We solve this model using the dynamical mean-field theory (DMFT). We adopt the generalized hybridization-expansion continuous-time quantum Monte Carlo method [43], in the implementation of Refs. [36,44] and [45], for solving the quantum impurity problem; more details are given in Supplemental Material [46]. We define the orbital polarization, the order parameter for OO, as $p(T) = (n_3 + n_2)/2 - n_1$, where n_i are the occupations of the natural orbitals, ordered such that $n_{i+1} \ge n_i$. The magnetization is $m(T) = (n_{\uparrow} - n_{\downarrow})/2$, where $n_{i\sigma} = \sum_{m} n_{im\sigma}$. The atomic-limit ground t_{2g}^2 multiplet is 3P , a spin and orbital triplet. The orbital triplet states can be written as $|\bar{m}_3\rangle = |m_1 m_2\rangle$, where $m_1 \neq m_2$ are the occupied orbitals and \bar{m}_3 the empty orbital, with $m_i \in \text{span}(xy, xz, yz)$ [30]. Using this notation, the hole orbital at site i is

$$|\theta,\phi\rangle_{\alpha}^{i} = \sin\theta\cos\phi|xz\rangle + \cos\theta|xy\rangle + \sin\theta\sin\phi|yz\rangle.$$
 (2)

In the GdFeO₃-type structure, there are four (equivalent) V sites in the unit cell. The reference site is i=1, and for simplicity we set $|\theta,\phi\rangle_{\alpha}^1=|\theta,\phi\rangle_{\alpha}$; the hole orbitals for the remaining sites are constructed by symmetry [47]. The label α in Eq. (2) specifies how the state is obtained: $|\theta,\phi\rangle_{\rm OO}$, from LDA + DMFT calculations for the experimental structure; $|\theta,\phi\rangle_{\rm KK}$, from LDA + DMFT calculations for an idealized structure with no CF splitting; $|\theta,\phi\rangle_{\rm M}$, maximizing the SE total energy gain (see next section). Finally, the highest energy CF state is $|\theta,\phi\rangle_{\rm CF}$.

Superexchange Hamiltonian—The crucial element of the puzzle is the materials-specific SE Hamiltonian [31]. Recently we introduced a systematic approach to build it from (1) via irreducible-tensor decomposition [30,35]. This yields $\hat{H}_{SE} = \frac{1}{2} \sum_{ij} \hat{H}_{SE}^{i,j}$, with

$$\hat{H}_{SE}^{i,j} = \sum_{aa'} \sum_{\nu\nu'} \sum_{rr'} \sum_{uu'} \hat{\tau}_i^{r\mu;q\nu} D_{r\mu,r'\mu'}^{ij;q\nu} \hat{\tau}_j^{r'\mu';q\nu}, \qquad (3)$$

where r = 0, 1, 2 is the orbital rank (monopole, dipole, quadrupole) with components $\mu = -r, ..., r$, and q = 0, 1 (monopole, dipole) is the spin rank with components $\nu = -q, ..., q$. It is convenient to split Eq. (3) as

$$\hat{H}_{\rm SE}^{i,j} = \hat{H}_{C_{ij}} + \hat{H}_{O_iO_j} + \hat{H}_{S_iS_j} + \hat{H}_{S_iS_jO_iO_j}. \tag{4}$$

The first term, $\hat{H}_{C_{ii}}$, obtained by setting r = r' =q = q' = 0, in the absence of charge ordering, is a constant, independent on the orbital and spin state; here we take it as the energy zero. The second term, $\hat{H}_{O_iO_i}$, obtained by setting q = 0 and $r + r' \neq 0$, describes the interaction between orbital pseudospins, independent of the magnetic state. The third term $(r = r' = 0 \text{ and } q \neq 0)$ describes a pure spin-spin interaction, independent of the orbital state. Finally the last term, obtained for $r + r' \neq 0$, q = 1, is $\hat{H}_{S:S:O:O:}$, and describes the entangling of spins and orbitals. The analytic expressions of the tensor elements $D_{ru,r'u'}^{ij;q\nu}$ can be found in Ref. [30]. They depend on U,J, and the hopping integrals; the latter are listed in Supplemental Material [46]. From Eq. (3) we calculate $\Delta E(\theta, \phi)$, the SE energy for a given spin and orbital ordering; minimizing it yields $|\theta,\phi\rangle_{\rm M}$. Finally, in order to unravel the mechanism behind the emergent ordering, we resort to a novel scheme: we decompose the order parameter itself into its irreducible components, $p_q = \sum_{r>0\mu} a_{r\mu;q0} \langle \hat{ au}_i^{r\mu;q0} \rangle$; the orbital polarization is $p = p_0$, while $m = \langle \hat{\tau}_i^{00;10} \rangle$. Last, the expectation value of an operator for a specific hole orbital [48] is $\langle \hat{\tau}_i^{r,\mu} \rangle_{\alpha} =_{\alpha} \langle \theta, \phi | \hat{\tau}_i^{r,\mu;q\nu} | \theta, \phi \rangle_{\alpha}$.

Orbital ordering in the paramagnetic phase—In Fig. 2, panel (a), we show the orbital polarization, p(T), in the paramagnetic (PM) phase; the corresponding hole orbital is $|\theta,\phi\rangle_{\rm OO}$. We define $T_{\rm OO}$ as the temperature for which

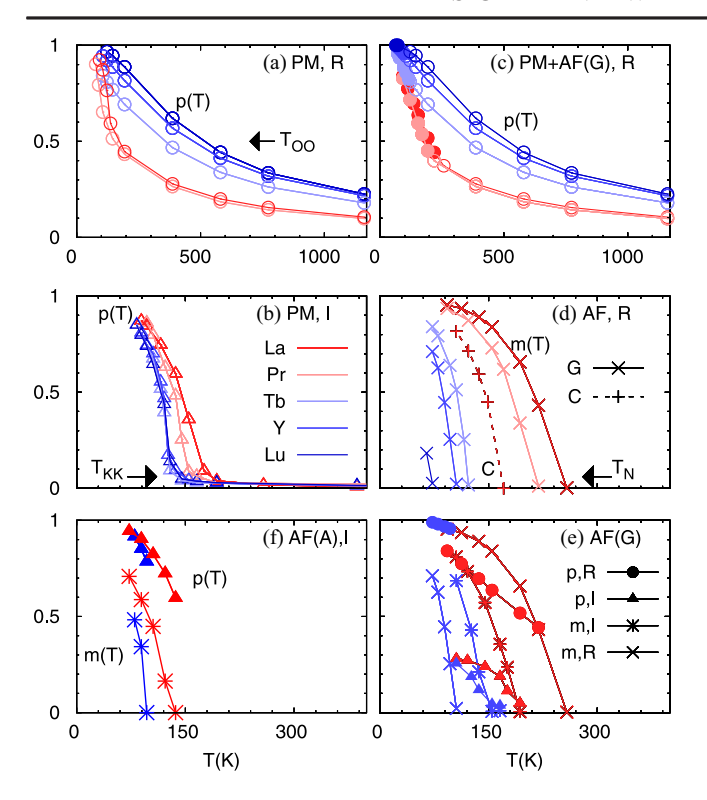


FIG. 2. Orbital and magnetic transitions in the RVO_3 series. Order parameters: p(T) (orbital polarization), panels (a), (b), (c) and (f), and m(T) (magnetic moment), panels (d), (e) and (f). Open symbols: p(T), paramagnetic (PM) phase. Filled symbols: p(T), AF phase. I: idealized case with no CF splitting. R: experimental structure; T_{OO} : temperature yielding p=0.5 (corresponding to the jump in p(T) in case I). AF: antiferromagnetic of G, C, A type.

p(T) = 0.5, i.e., for which orbital fluctuations are sizably suppressed. The figure shows that $T_{\rm OO}$ is appreciably higher for $R = {\rm Lu}$ than for $R = {\rm La}$. These calculations

include both SE and lattice distortion effects. In order to single out SE effects from the rest, we repeat the same calculations but this time for $\varepsilon_{\rm CF}=0$, panel (b); this yields $T_{\rm KK}$, the SE transition temperature, and the associated hole orbital, $|\theta,\phi\rangle_{\rm KK}$. The figure shows that $T_{\rm KK}$ increases going from Tb to La, with a variation of at most 60 K, i.e., $T_{\rm KK}$ behaves the *opposite* of $T_{\rm OO}$.

The trend for $T_{\rm KK}$ can be understood from Fig. 3, bottom panel. It shows the SE energy, $\Delta E(\theta,\phi)$, split into its irreducible-tensor components, for the ideal case $|\theta,\phi\rangle=|\theta,\phi\rangle_{\rm M}$, the state that maximizes the SE energy gain (empty triangles). For small R_I the main contribution is from the anisotropic dipolar term (x,z). Increasing R_I , however, the weight shifts progressively to the quadrupolar (xz,xz) channel; this is because the GdFeO₃-type distortion decreases [42], which, *ceteris paribus*, reduces off-diagonal hopping integrals (see Supplemental Material [46]). This makes SE more efficient: the maximum energy gain in the (x,z) channel is for states not in line with lattice symmetry [47]. This explains the trends for $T_{\rm KK}$ in Fig. 2: indeed, when CF effects are negligible, $|\theta,\phi\rangle_{\rm KK} \sim |\theta,\phi\rangle_{\rm M}$.

The trend of $T_{\rm OO}$ is more complex to unravel. In the real structures, CF and SE energies are comparable, and the SE energy surface alone is not sufficient. To make progress, we decompose the order parameter p(T) into its irreducible components, $\langle \hat{\tau}_i^{r\mu;q\nu} \rangle$. The results are shown in Fig. 4, bottom panels (q=0). For small R_I , all components rise smoothly: there is no phase transition; the signature of SE interactions is merely small deviations of the saturation moments from the CF expectation values (filled squares). Increasing R_I , however, a sudden change of behavior occurs: a phase transition appears in the xz channel, very similar to the one obtained in the ideal case with no CF splitting (empty triangles) [46]. The (xz, xz) interaction is here the dominant one, as in the ideal case. This provides

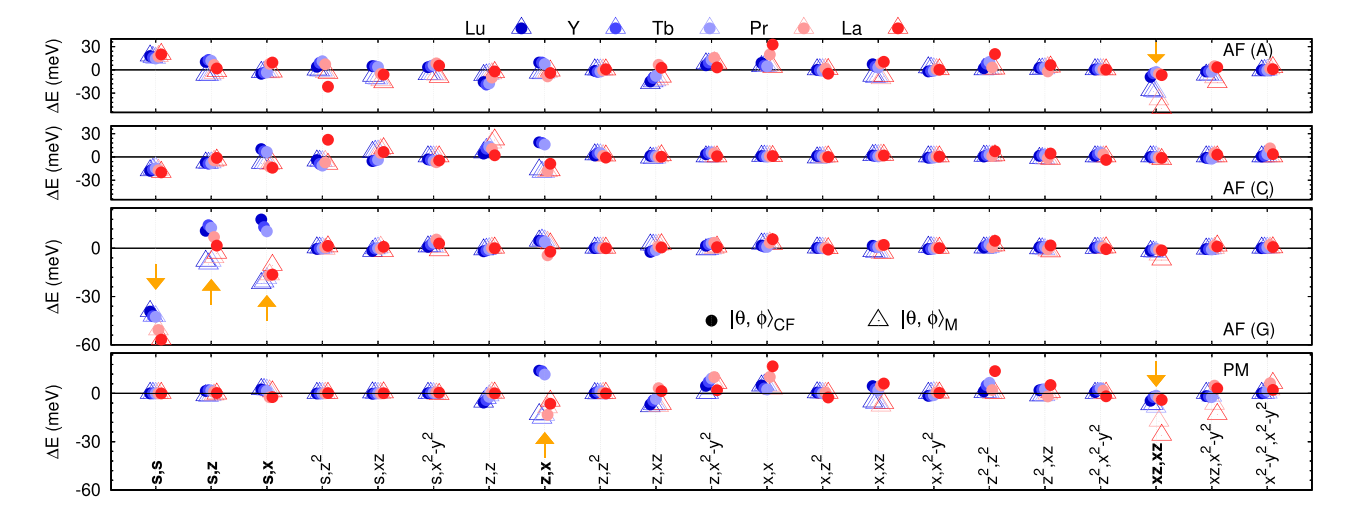


FIG. 3. SE energy gain $\Delta E(\theta, \phi)$ decomposed in irreducible tensor components for hole orbitals $|\theta, \phi\rangle_{CF}$ (filled circles) and $|\theta, \phi\rangle_{M}$, (empty triangles). From top to bottom: AF (A type), AF (C type), AF (G type), and PM case. Most terms give a very small contribution. The key terms (see main text) are bold and indicated by an arrow in each case.

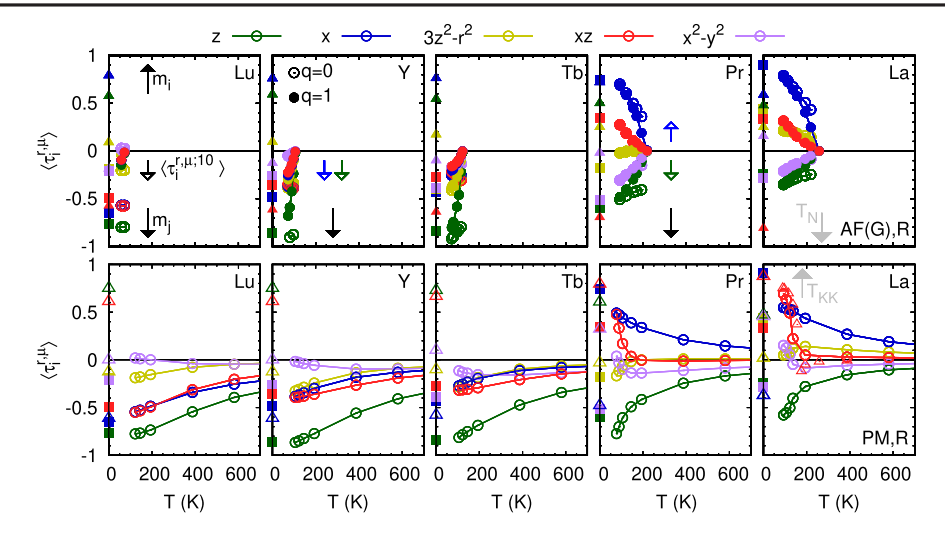


FIG. 4. Irreducible components of the order parameter, $\langle \hat{\tau}_i^{r\mu,q\nu} \rangle$, normalized to the maximum value they can reach [46]. T=0 axis: $\langle \theta, \phi | \hat{\tau}_i^{r,\mu,q\nu} | \theta, \phi \rangle_{\alpha}$ for $\alpha=M$ (triangles) and $\alpha=CF$ (filled square). Bottom: PM phase (empty symbols). Top: AF (G) (filled symbols). The magnetization is $m_i=m>0$ at site i (Fig. 2) and $m_i=-m$ at a neighboring site.

the key for explaining the trends. Starting from small R_I , the evolution of $T_{\rm OO}$ with increasing R_I essentially reflects the CF: $T_{\rm OO}$ decreases because the CF splitting decreases. Eventually, $T_{\rm OO} \sim T_{\rm KK}$, but this happens only for large R_I . This explains the opposite behavior of $T_{\rm OO}$ and $T_{\rm KK}$ with increasing R_I .

The resulting theoretical phase diagram for the PM phase is shown in Fig. 1, where the experimental structural transition T_S is also reported. The figure shows that $T_{\rm OO} > T_S$ for small R_I , while $T_{\rm OO} \sim T_S$ for large R_I . Correspondingly, for small R_I , right above T_S the polarization is large $(p(T) \gtrsim 0.75)$, i.e., OO is already well developed. Finally, $T_{\rm KK} < T_S$ for small R_I , while $T_{\rm KK} \sim T_{\rm OO} \gtrsim T_S$ for large R_I . Entering the monoclinic phase modifies the OO state, not the overall picture; it slightly enhances $T_{\rm KK}$, but the CF increases as well.

Antiferromagnetic phase—Finally, we turn to the surprising inversion of T_N and $T_{\rm OO}$ with increasing R_I . In the large R_I limit, G-type magnetic fluctuations, AF in all directions, are the first to appear on lowering the temperature [10]. Thus we start from the results for the G-type structure. Figure 2 shows that T_N [panel (d)], increases with R_I , similarly to $T_{\rm KK}$ [panel (b)], but much more rapidly. Thus, remarkably, our numerical calculations do yield $T_N < T_{\rm KK} < T_{\rm OO}$ for small R_I and $T_N > T_{\rm KK} \sim T_{\rm OO}$ for large R_I , in line with experiments.

Next, we explain why. Our decomposition of the SE interaction makes clear that the only interaction that can lead to $T_N > T_{\rm KK}$ is the r=0 (orbital monopolar) dipolar spin-spin term, (s,s). The latter, by itself, depends little on OO or the CF. We find that, furthermore, it is AF in all directions, and it is the dominant interaction; see Fig. 3. Its strength increases with R_I , in particular along ${\bf c}$, i.e., it is weaker for small R_I ; in the ideal case with no CF, it is just strong enough to make T_N slightly larger than $T_{\rm KK}$ for all

 R_I ; see Fig. 2, panel (e). It is only when we switch on the CF splitting, that we obtain the inversion of T_N and T_{KK} with increasing R_I .

This surprising effect is a consequence of the spin-orbital coupling via the $\hat{H}_{S_iS_jO_iO_j}$ SE term. Figure 4, top panel, shows that the q=1 and q=0 operators with r+r'>1 have similar expectation value below T_N . Thus, their contributions tend to cancel each other for AF order; see Fig. 3, AF(G) panel, for the limit of full magnetization. The channels influencing T_N , besides the dipole-dipole one (q=1,r=0), are thus mostly (s,μ) terms with spin rank q=1 and $\mu=x$, z. However, for small (but not for large) R_I , the latter, on a site i, yield moments parallel to the magnetization m_j on a neighbor j; see arrows in Fig. 4; the associated frustration reduces T_N . This is why, for the real structures, $T_N > T_{KK} \sim T_{OO}$ for large R_I but $T_N < T_{KK} < T_{OO}$ when R_I is small.

Let us now consider other possible AF magnetic structures: C type, with ferro (F) order along c, found in the monoclinic phase, and A-type, with F order in the ab plane, not found experimentally in the series. In both these structures, for at least one bond the (s, s) component of the spin-spin interaction is frustrated. This, taken alone, reduces T_N . The F stacking, either along c or in the plane, is stabilized by terms with orbital rank r + r' > 0, hence by OO, however. For La, Fig. 2 shows that indeed $T_N \sim T_{\rm KK} \sim T_{\rm OO}$ for C-type magnetic order. Entering the monoclinic phase, ceteris paribus, does not change this conclusion: the (s, s) magnetic term remains in fact essentially the same; C-type spin order is assisted by the CF splitting [49]. Finally, in the A phase, there is no magnetic order without OO for the systems considered, since the (s, s) spin-spin orbital monopolar interaction alone gives an energy loss; see Fig. 2, panel (f).

Conclusion—In this Letter, augmenting DMFT with a new analysis scheme based on the decomposition of the

order parameter into its irreducible components, we explain the origin of the T_N - T_{OO} inversion in the vanadates. This has consequences beyond the RVO₃ series. In fact, our results clarify why the inversion is rare: in most orbitally ordered systems T_{OO} is determined by lattice distortions, i.e., $T_{\rm OO} \gg T_{\rm KK}$. This in turn explains why unconventional quantum orbital phases are usually suppressed. The inversion instead requires, at the same time, that (i) $T_{\rm OO} \sim T_{\rm KK}$, and (ii) the magnetic structure is mostly determined by dipolar interactions with orbital rank r = 0. Furthermore, the nature of the inversion, unraveled here, makes systems potentially hosting it an ideal playground for studying quantum orbital phases, at the same time providing criteria for finding more systems of that kind. Moreover, the order parameter decomposition should prove a powerful tool for understanding other classes of problems, such as the nature of octupolar order in materials with strong spin-orbit coupling.

Acknowledgments—We would like to acknowledge computational time on the supercomputer JURECA [50], Forschungszentrum Jülich, and the GCS [51] supercomputer JUWELS through NIC at Jülich Supercomputing Centre.

- [1] D. I. Khomskii, *Transition Metal Compounds* (Cambridge University Press, Cambridge, England, 2014).
- [2] Y. Tokura and N. Nagaosa, Science 288, 462 (2000).
- [3] E. Dagotto, Science 309, 257 (2005).
- [4] H. Y. Hwang, Y. Iwasa, M. Kawasaki, B. Keimer, N. Nagaosa, and Y. Tokura, Nat. Mat. 11, 103 (2012).
- [5] J. Yan, A. Kumar, M. Chi, M. Brahlek, T. Z. Ward, and M. A. McGuire, Phys. Rev. Mater. 8, 024404 (2024).
- [6] A. S. Disa, J. Curtis, M. Fechner, A. Liu, A. von Hoegen, M. Först, T. F. Nova, P. Narang, A. Maljuk, A. V. Boris, B. Keimer, and A. Cavalleri, Nature (London) 617, 73 (2023).
- [7] P. Horsch, A. M. Oleś, L. F. Feiner, and G. Khaliullin, Phys. Rev. Lett. 100, 167205 (2008).
- [8] M. J. Martínez-Lope, J. A. Alonso, M. Retuerto, and M. T. Fernández-Díaz, Inorg. Chem. 47, 2634 (2008).
- [9] J.-S. Zhou, Y. Ren, J.-Q. Yan, J. F. Mitchell, and J. B. Goodenough, Phys. Rev. Lett. 100, 046401 (2008).
- [10] Y. Ren, A. A. Nugroho, A. A. Menovsky, J. Strempfer, U. Rütt, F. Iga, T. Takabatake, and C. W. Kimball, Phys. Rev. B 67, 014107 (2003).
- [11] J.-Q. Yan, J.-S. Zhou, and J. B. Goodenough, Phys. Rev. Lett. **93**, 235901 (2004).
- [12] M. H. Sage, G. R. Blake, G. J. Nieuwenhuys, and T. T. M. Palstra, Phys. Rev. Lett. 96, 036401 (2006).
- [13] P. N. Shanbhag, F. Fauth, and A. Sundaresan, Phys. Rev. B 108, 134115 (2023).
- [14] M. Nasir, I. Kim, Ki. Lee, S. Kim, K. Hyoung Lee, and H. Jung Park, Phys. Chem. Chem. Phys. 25, 3942 (2023).
- [15] H. Meley, M. Tran, J. Teyssier, J. A. Krieger, T. Prokscha, A. Suter, Z. Salman, M. Viret, D. van der Marel, and S. Gariglio, Phys. Rev. B 103, 125112 (2021).

- [16] J.-Q. Yan, W. Tian, H. B. Cao, S. Chi, F. Ye, A. Llobet, A. Puretzky, Q. Chen, J. Ma, Y. Ren, J.-G. Cheng, J.-S. Zhou, M. A. McGuire, and R. J. McQueeney, Phys. Rev. B 100, 184423 (2019).
- [17] E. Benckiser, L. Fels, G. Ghiringhelli, M. Moretti Sala, T. Schmitt, J. Schlappa, V. N. Strocov, N. Mufti, G. R. Blake, A. A. Nugroho, T. T. M. Palstra, M. W. Haverkort, K. Wohlfeld, and M. Grüninger, Phys. Rev. B 88, 205115 (2013).
- [18] F. Novelli, D. Fausti, J. Reul, F. Cilento, P. H. M. van Loosdrecht, A. A. Nugroho, T. T. M. Palstra, M. Grüninger, and F. Parmigiani, Phys. Rev. B **86**, 165135 (2012).
- [19] K. Ruotsalainen, M. Gatti, J. M. Ablett, F. Yakhou-Harris, J.-P. Rueff, A. David, W. Prellier, and A. Nicolaou, Phys. Rev. B 103, 235158 (2021).
- [20] M. H. Sage, G. R. Blake, C. Marquina, and T. T. M. Palstra, Phys. Rev. B 76, 195102 (2007).
- [21] G. R. Blake, T. T. M. Palstra, Y. Ren, A. A. Nugroho, and A. A. Menovsky, Phys. Rev. Lett. 87, 245501 (2001).
- [22] M. Reehuis, C. Ulrich, K. Prokeš, S. Matáš, J. Fujioka, S. Miyasaka, Y. Tokura, and B. Keimer, Phys. Rev. B 83, 064404 (2011).
- [23] R. Saha, F. Fauth, V. Caignaert, and A. Sundaresan, Phys. Rev. B 95, 184107 (2017).
- [24] M. Reehuis, C. Ulrich, P. Pattison, M. Miyasaka, Y. Tokura, and B. Keimer, Eur. Phys. J. B 64, 27 (2008).
- [25] S. Miyasaka, Y. Okimoto, M. Iwama, and Y. Tokura, Phys. Rev. B 68, 100406(R) (2003).
- [26] J.-S. Zhou, J. B. Goodenough, J.-Q. Yan, and Y. Ren, Phys. Rev. Lett. 99, 156401 (2007).
- [27] A. Munoz, J. A. Alonso, M. T. Casáis, M. J. Martínez-Lope, J. L. Martínez, and M. T. Fernández-Díaz, Phys. Rev. B 68, 144429 (2003).
- [28] J. Reul, A. A. Nugroho, T. T. M. Palstra, and M. Grüninger, Phys. Rev. B 86, 125128 (2012).
- [29] M. De Raychaudhury, E. Pavarini, and O. K. Andersen, Phys. Rev. Lett. 99, 126402 (2007).
- [30] X.-J. Zhang, E. Koch, and E. Pavarini, Phys. Rev. B **105**, 115104 (2022).
- [31] K. I. Kugel and D. I. Khomskii, Zh. Eksp. Teor. Fiz. 64, 1429 (1973) [Sov. Phys. JETP 37, 725 (1973)].
- [32] X.-J. Zhang, E. Koch, and E. Pavarini, Phys. Rev. B **106**, 115110 (2022).
- [33] E. Pavarini, E. Koch, and A. I. Lichtenstein, Phys. Rev. Lett. **101**, 266405 (2008).
- [34] E. Pavarini and E. Koch, Phys. Rev. Lett. **104**, 086402 (2010).
- [35] X.-J. Zhang, E. Koch, and E. Pavarini, Phys. Rev. B 102, 035113 (2020).
- [36] J. Musshoff, G. Zhang, E. Koch, and E. Pavarini, Phys. Rev. B 100, 045116 (2019).
- [37] C. Autieri, E. Koch, and E. Pavarini, Phys. Rev. B 89, 155109 (2014).
- [38] P. Blaha, K. Schwarz, P. Sorantin, and S. Trickey, Comput. Phys. Commum. **59**, 399 (1990).
- [39] N. Marzari and D. Vanderbilt, Phys. Rev. B **56**, 12847 (1997).
- [40] A. A. Mostofi, J. R. Yates, Y.-S. Lee, I. Souza, D. Vanderbilt, and N. Marzari, Comput. Phys. Commun. 178, 685 (2008); J. Kuneś, R. Arita, P. Wissgott,

- A. Toschi, H. Ikeda, and K. Held, Comput. Phys. Commun. **181**, 1888 (2010).
- [41] T. Mizokawa and A. Fujimori, Phys. Rev. B 54, 5368 (1996).
- [42] E. Pavarini, A. Yamasaki, J. Nuss, and O. K. Andersen, New J. Phys. 7, 188 (2005).
- [43] E. Gull, A. J. Millis, A. I. Lichtenstein, A. N. Rubtsov, M. Troyer, and P. Werner, Rev. Mod. Phys. 83, 349 (2011).
- [44] A. Flesch, E. Gorelov, E. Koch, and E. Pavarini, Phys. Rev. B **87**, 195141 (2013).
- [45] J. Musshoff, A. Kiani, and E. Pavarini, Phys. Rev. B 103, 075136 (2021).
- [46] See Supplemental Material at http://link.aps.org/supplemental/10.1103/qvp2-jn9p for further details, hopping integrals, and energy landscapes.
- [47] We define V_1 and V_2 two neighboring sites in one layer and V_3 and V_4 the corresponding ones in the layer above, with

- V_3 on top of V_1 , in the GdFeO₃-type structure; if $|\theta,\phi\rangle^1$ is the hole orbital at site V_1 , the hole orbitals at the other sites are $|\theta,\phi\rangle^2=|\theta,(\pi/2)-\phi\rangle^1$, $|\theta,\phi\rangle^3=|-\theta,\phi\rangle^1$, and $|\theta,\phi\rangle^4=|-\theta,(\pi/2)-\phi\rangle^1$, respectively. In the monoclinic case, $|\theta,\phi\rangle^3\sim|-\theta-\delta_\theta,\phi\pm\delta_\phi\rangle$ maximizes the energy gain for $\delta_\theta\sim 20^\circ$ and $\delta_\phi\sim 110^\circ$ in the PM phase.
- [48] For a given spin rank q, there are only two independent saturation $(T \to 0)$ values. This is because, for a specific hole orbital, $\langle \hat{\tau}_i^{r,\mu} \rangle_{\alpha} = \langle \theta, \phi | \hat{\tau}_i^{r,\mu;q\nu} | \theta, \phi \rangle_{\alpha}$, depend on two variables only, θ and ϕ [46]. These constraints do not hold at finite temperature, however.
- [49] The CF can affect T_N more for C-type than G-type magnetic order.
- [50] Jülich Supercomputing Centre, J. Large-Scale Res. Facil. 7, A182 (2021).
- [51] www.gauss-centre.eu